Water Practice & Technology

IWA PUBLISHING

Water Practice & Technology Vol 18 No 11, 2785 doi: 10.2166/wpt.2023.182

Chromium (VI) and lead (II) adsorption using *Mangifera kemanga* leaves

Dian Arrisujaya [a,*], Niti Sae Utami[a], Tia Mulyawati[a], Dea Rahmalisa[a], Siska Wati[a] and Hidayat Hidayat[b]

[a] Department of Chemistry, Faculty of Mathematics and Natural Sciences, Universitas Nusa Bangsa, Bogor 16166, Indonesia
[b] Research Unit for Clean Technology, National Research and Innovation Agency, Bandung 40135, Indonesia
*Corresponding author. E-mail: arrisujaya@unb.ac.id

DA, 0000-0002-9053-756X

ABSTRACT

This work reports the use of *Mangifera kemanga* leaves (MKL) treated with ethanol and nitric acid as an adsorbent to remove Cr(VI) and Pb(II) ions at different pHs, adsorbent dosages, times, initial metal ion concentrations, and temperatures. The MKL's maximum adsorption capacity was 213 mg/g for Cr(VI) at pH 2 and 89 mg/g for Pb(II) at pH 6. Batch experiments showed that MKL follows the Langmuir isotherm model in absorbing Cr(VI) and Pb(II). The Cr(VI) and Pb(II) adsorption kinetics are best suited by the pseudo-second-order kinetics model. Thermodynamic data studies indicated that surface complexation coexisted with ion exchange as the preliminary removal means. The results implied that MKL could potentially remove Cr(VI) and Pb(II).

Key words: adsorption, biosorbent, heavy metals, Kemang, leaves, removal

HIGHLIGHTS

- Kemang leaves were used as biosorbent for Cr(VI) and Pb(II) removal from aqueous solution.
- The biosorption capacity of the biosorbent for Cr(VI) was 212.76 mg/g.
- The biosorption capacity of the biosorbent for Pb(II) was 89.29 mg/g.
- Both Cr(VI) and Pb(II) adsorption were well suited by a pseudo-second-order model.
- Biosorbent may be regenerated and reused, indicating materials' economic benefits.

1. INTRODUCTION

Surface water pollution is important globally. Unfortunately, industrialization and irresponsible industrial practices have resulted in severe environmental damage and contamination of ecosystems (Nkutha *et al.* 2021). Toxic pollutants from industrial operations have contaminated surface waters, damaged many ecosystems, and caused severe health issues worldwide (Azizi *et al.* 2023).

Cr(VI) and Pb(II) harm living organisms and do not biodegrade (Shooto 2020). Unfortunately, these pollutants are present in freshwater resources due to careless discharge by mines, metal plating, metallurgy and chemical industries, and factories that produce plastics, paper, fertilizers, pesticides, batteries, etc. (Ali *et al.* 2019; Emamy *et al.* 2021; Nkutha *et al.* 2021).

When heavy metals are discharged without proper treatment, they can harm ecosystems due to their high reactivity with plants and animals. High concentrations of Cr(VI) can be harmful to human health since it is both carcinogenic and teratogenic (Lala *et al.* 2023) because it can penetrate cells, resulting in health problems like skin itch and gastric damage, and harm to essential organs such as the liver, kidneys, and lungs (Shooto 2020). Exposure to lead has also been linked to interference in the developing nervous systems of young juveniles, which can cause dyslexia, mental impairment, attention deficit disorder, and antisocial behavior (Lim *et al.* 2019).

Recently, different methods have been studied for treating water contaminated by heavy metals. Conventional technologies include ion exchange, chemical precipitation, biological treatment, electrochemistry, membrane filtration, and adsorption to remove Cr(VI) and Pb(II) from the solution. Adsorption involves using an adsorbent to remove these ions through ion exchange, complexation, and adsorption (Azizi *et al.* 2023), which offers low cost,

energy consumption, and environmental impact, with high efficiency and ability to regenerate briefly (Arrisujaya *et al.* 2019).

Various agriculture-based materials have been used as adsorbents for the removal of Cr(VI) and Pb(II) ions recently, including Sweet flag (Shooto 2020), *Juniperus procera* leaves (Ali *et al.* 2019), green tea leaves (Jeyaseelan & Gupta 2016), *Diospyros discolor* seed (Arrisujaya *et al.* 2019), areca nut leaf sheath (Pant *et al.* 2022), sugar palm fruit shells (Nazaruddin *et al.* 2014), *Terminalia catappa* shell (Hevira *et al.* 2020), rice husk (Lala *et al.* 2023), *Hura crepitans* (Abadi *et al.* 2023), Pomelo leaves (Lim *et al.* 2019), *Lawsonia inermis* (Mehrmand *et al.* 2022), and pineapple fiber (Tangtubtim & Saikrasun 2019) to remove metal ions. These materials are plentiful, cheap, reasonable, reusable, and safe in the environment for living beings and the ecosystem (Shooto 2020). The biosorbents were created using plant components and natural resources with functional groups like hydroxyl, aldehyde, amine, amide, and aliphatic acid (Arrisujaya *et al.* 2020; Hevira *et al.* 2020).

Kemang (*Mangifera kemanga* Blume) is a member of the Anacardiaceae family and grows naturally along rivers in Java, especially West Java, Indonesia. Different parts of the plant exhibit antioxidant, anti-degenerative, and anticancer properties due to active chemical components such as flavonoids, tannins, triterpenoids, alkaloids, and phenylpropanoids (Darsono *et al.* 2022). The use of *M. kemanga* Blume for wastewater treatment has yet to be widely studied. Previous research indicated that kemang seeds were reliable for removing phenol (Mardiah *et al.* 2022), but further investigation is needed to determine their effectiveness in removing other pollutants, including heavy metals. This study examines the adsorption capacity of *M. kemanga* leaves (MKLs) in removing Cr(VI) and Pb(II) ions from water solutions.

2. MATERIALS AND METHODS

2.1. Materials

MKLs were obtained from local communities' plantations in Cijayanti-Bogor, Indonesia. A stock solution of Cr(VI) and Pb(II) was made by dissolving $K_2Cr_2O_7$ and $Pb(NO_3)_2$ in double-distilled water. All solutions were made with double-distilled water and other analytical-grade chemicals such as HNO_3, HCl, and NaOH. An atomic absorption spectrophotometer (AA-7000 Shimadzu) was used to measure the concentration of Cr(VI) and Pb(II) before and after contact with the adsorbent.

2.2. Enhanced MKLs

The leaves were rinsed in distilled water repeatedly to eliminate dissolved impurities and dirt particles and dried for 24 h in an air oven at 333 K. They were then dried, ground, and sieved using a 100 mesh sieve to obtain a homogeneous particle size. The uniform fine powder was steeped and agitated in ethanol (96%) for 2 h (Arrisujaya *et al.* 2019; Mardiah *et al.* 2022), then activated in 0.01 mol L nitric acid for 2 h at room temperature (Hevira *et al.* 2020).

2.3. Batch adsorption studies

The MKL biosorbent (1 g) was added to the adsorbate solution (100 mL Cr(VI) or Pb(II) ions) in 100 mL Erlenmeyer flasks. They were shaken at 125 rpm for 30 min to establish equilibrium. The adsorption controlling parameter was determined by altering the initial pH (2, 3, 4, 5, and 6), using an Ohaus Starter 3100 pH meter; the adsorbent dosage (1, 2, 3, and 4 g/L); contact time (30, 60, 90, and 120 min); and adsorbate concentration (50, 100, 150, and 200 mg/L). Finally, the adsorbate-mixed solution was filtered using paper.

The adsorption capacity (q_e (mg/g)) of Cr(VI) and Pb(II) onto the MKL biosorbent at equilibrium is determined using Equation (1):

$$q_e = \frac{(C_0 - C_e)}{m} \times V \tag{1}$$

where C_0 and C_e are the initial and equilibrium concentrations of the adsorbate (mg/L), respectively, V represents the adsorbate solution volume added (L), and m is the mass of the MKL biosorbent (g).

To conduct the kinetic studies, a sequence of varying initial concentrations (50, 100, and 150 mg/L) of the adsorbate solution was used. The adsorption capacity onto the biosorbent (q_t (mg/g)) is determined

using Equation (2):

$$q_t = \frac{(C_0 - C_t)}{m} \times V \tag{2}$$

where C_t is the adsorbate solution concentration at any time t (mg/L).

The equilibrium isotherm studies used the Langmuir, Freundlich, Temkin, and Dubinin–Radushkevich isotherms. The kinetics studies were based on three models: pseudo-first-order, pseudo-second-order, and intraparticle diffusion. The Van't Hoff Equation was used for thermodynamic analysis.

2.4. Desorption studies

The MKL biosorbent used previously for the Cr(VI) and Pb(II) adsorption of an initial metal concentration of 100 mg/L was separated from the adsorbate solution by filter paper. The adsorbate-loaded MKL was agitated for 2 h with 100 mL of 0.01 mol L HNO_3 solution. Desorption efficiency E_d is defined in Equation (3).

$$E_d = \frac{Q_d}{Q_e} \times 100\% \tag{3}$$

where Q_d and Q_e are the amount of metal desorbed and loaded (mg), respectively.

3. RESULTS AND DISCUSSION

3.1. Effect of pH

The level of acidity or alkalinity in an aqueous solution plays a crucial role in metal ion adsorption. The effect of pH on the Cr(VI) and Pb(II) adsorption onto MKL is shown in Figure 1(a), with Cr(VI) adsorption capacity falling as the pH rises from 2 to 6. Similar decreasing trends have previously been observed in research on heavy metal adsorption onto several biosorbents (Emamy *et al.* 2021; Nkutha *et al.* 2021; Azizi *et al.* 2023). In acidic pH conditions, Cr(VI) ions behave as anions ($HCrO_4^-$, CrO_4^{2-}, or $Cr_2O_7^{2-}$), and protonation occurs on the binding sites on the MKL biosorbent surface (Arrisujaya *et al.* 2019). The surface of the MKL biosorbent carries a considerable positive charge, strengthening the electrostatic interactions between binding sites on the MKL biosorbent and Cr(VI) ions (Pant *et al.* 2022). The MKL's protonated surface diminishes steadily with increasing pH, suggesting that the anions (OH^-, $HCrO_4^-$, CrO_4^{2-}, and $Cr_2O_7^{2-}$) compete for adsorption, resulting in a decrease in Cr(VI) adsorption capacity (Arrisujaya *et al.* 2019; Lala *et al.* 2023).

In contrast, Pb(II) adsorption capacity increased to about 29 mg/g from about 7 as the initial solution pH rose from 2 to 6 – i.e., MKL's Pb(II) adsorption capacity is more effective in an average acidic solution than in a strong one (Emamy *et al.* 2021; Nkutha *et al.* 2021). The effect of solution pH on Pb(II) adsorption might arise from competition on the protonated MKL surface between protons (H^+) and Pb(II) cations, resulting in lower polarity (Shooto 2020). Protonation decreases as pH increases, and the OH^- groups increase in conjunction with the more prominent deprotonated MKL surface, indicating a partial negative charge on the latter. Hence, the positively charged Pb(II) adsorption onto MKL increases through electrostatic interaction and surface complexation (Ali *et al.* 2019; Shooto 2020).

3.2. Biosorbent dosage

Cr(VI) and Pb(II) adsorptions onto MKLs were influenced considerably by biosorbent dosage (Figure 1(b)). Cr(VI) and Pb(II) adsorption capacity appeared to decrease with the MKL dosage increasing from 1 to 4 g/L. This could arise because more binding sites are available on the MKL surface (Hevira *et al.* 2020). At the same time, the Cr(VI) and Pb(II) initial concentrations are restricted to the value of 100 mg/L used in this study of the effect of the MKL biosorbent dosage.

3.3. Contact time

Contact time is an essential metric because it determines the period to achieve equilibrium and the optimum term for heavy metal ion adsorption. Figure 1(c) displays the time-dependent adsorption of Cr(VI) and Pb(II) onto MKL. The concentration of adsorbate increased and ultimately stabilized once it attained equilibrium. The physicochemical nature of the adsorption process was determined, and it was found to be unaffected by energy. It was further observed that the electrostatic forces played a crucial role in the process (Ali *et al.* 2019). Various steps

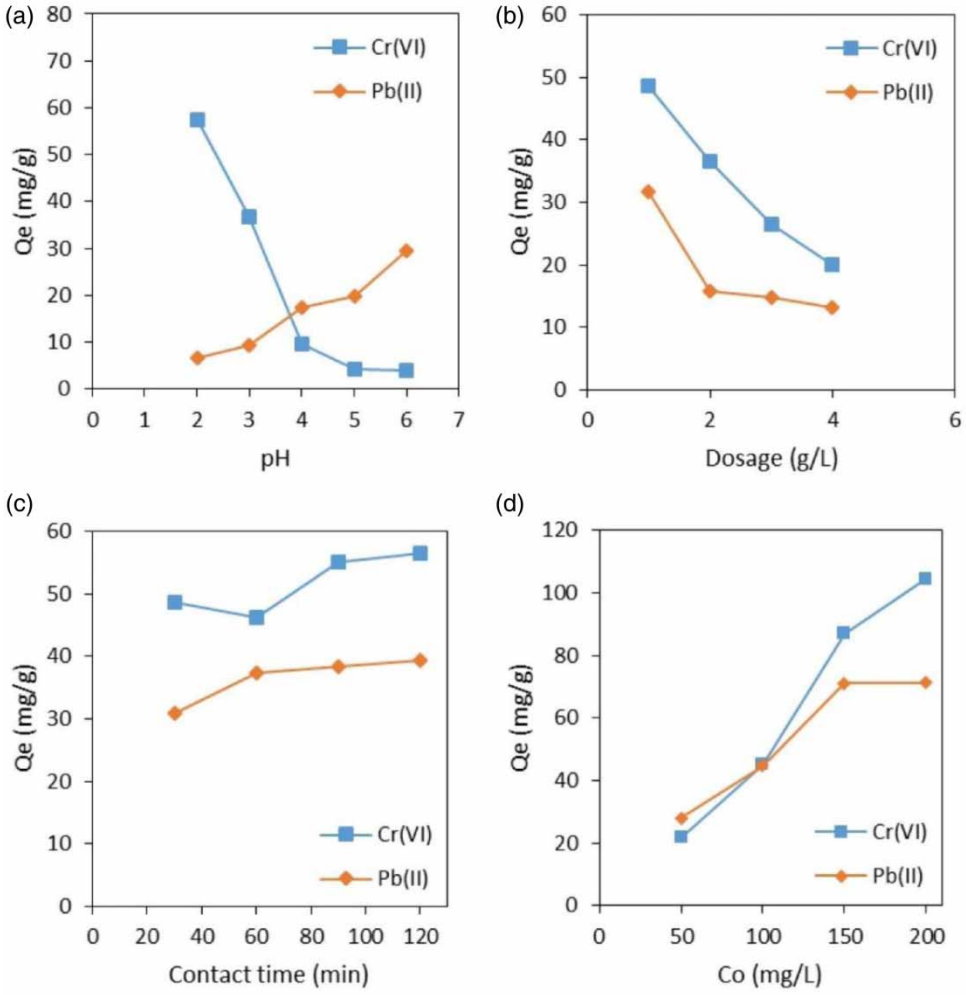

Figure 1 | Cr(VI) and Pb(II) adsorption controls onto MKL. (a): Adsorbate solution pH; (b) biosorbent dose; (c) contact time; and (d) initial adsorbate concentration.

can control adsorption, including film, external and intra-particle diffusion, and adsorption on the adsorbent surface (Lin *et al.* 2017). It was confirmed that equilibrium adsorption of Cr(VI) and Pb(II) arises at approximately 90 min, so, for all studies, 90-min adsorption contact time was used.

3.4. Initial adsorbate concentration

Adsorbate displacement, such as metal ions between the liquid and solid phases, heavily relies on their initial concentration. The effect of initial Cr(VI) and Pb(II) concentration on the MKL adsorbate was considered using standard 50, 100, 150, and 200 mg/L working solutions at 298 K and a 1 g/L adsorbent dose (Figure 1(d)). As the initial concentration was increased, MKL adsorbed more Cr(VI) and Pb(II), indicating a direct relationship between them. As the initial adsorbate solution concentration increased, MKL's adsorption ability increased – i.e., mass transfer was increased in solutions with elevated initial concentrations because there are more possibilities for metal ions to collide with binding sites (Lim *et al.* 2019) on the MKL surface. Cr(VI) and Pb(II) adsorption on MKL followed similar patterns (Figure 1(d)). The maximum Cr(VI) adsorption capacity on MKL from the 200 mg/L working solution was about 105 mg/g, while, for Pb(II), it was 71 mg/g – i.e., MKL removed Cr(VI) better than Pb(II).

3.5. Equilibrium isotherm modeling

MKL adsorption of Cr(VI) and Pb(II) was examined using four adsorption isotherm models such as Langmuir, Freundlich, Temkin, and Dubinin–Radushkevich. Adsorption isotherm models revealed the equilibrium distinction between adsorbate concentration in the solution and the concentration of adsorbate enclosed in the MKL

biosorbent at specific temperatures (Azizi *et al.* 2023). They could be plotted based on information on MKL biosorbent adsorption capacity versus the initial adsorbate concentration (Arrisujaya *et al.* 2019; Shooto 2020). The Langmuir isotherm model can be simplified to a linear form – Equation (4) – that applies to adsorption onto a surface with limited uniform sites:

$$\frac{1}{q_e} = \left[\frac{1}{K_L \cdot q_m}\right]\frac{1}{C_e} + \frac{1}{q_m} \tag{4}$$

where q_e is the adsorption capacity (mg/g) at equilibrium; q_m is the maximum adsorption capacity (mg/g); C_e is the adsorbate equilibrium concentration (mg/L); and K_L is the Langmuir adsorption equilibrium constant (L/mg). Figure 2(a) is a plot of $1/q_e$ versus $1/C_e$, illustrating Cr(VI) and Pb(II) adsorption onto the MKL surface. Table 1 shows the values of K_L and q_m values, which were calculated by the intercept and slope of the $1/q_e$ versus $1/C_e$. Additionally, the dimensionless constant separation factor (R_L) values, a fundamental attribute of the Langmuir isotherm, provide considerable evidence of sorption nature (Ali *et al.* 2019). This tool effectively clarifies the attractions and interactions between the sorbent and sorbate. The value of R_L is determined using Equation (5):

$$R_L = \frac{1}{1 + K_L C_0} \tag{5}$$

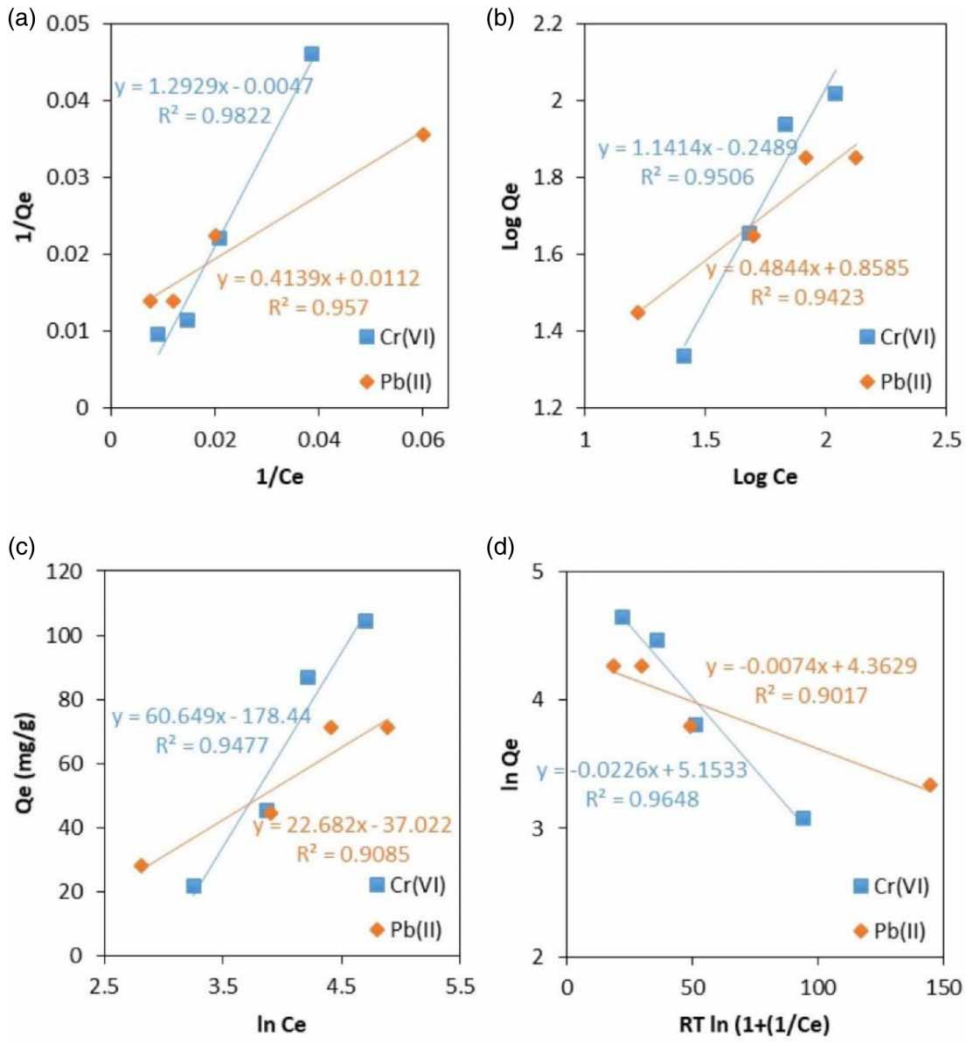

Figure 2 | Adsorption isotherm models for Cr(VI) and Pb(II) using MKL. (a) Langmuir; (b) Freundlich; (c) Temkin; and (d) Dubinin–Radushkevich.

Table 1 | Isotherm and desorption parameters for Cr(VI) and Pb(II) adsorption onto the MKL biosorbent

Isotherm parameters	Cr(VI)	Pb(II)
Langmuir isotherm		
q_{max} (mg/g)	212.76	89.29
K_L (L/mg)	0.0036	0.027
R^2	0.9822	0.957
Freundlich isotherm		
K_f	1.7737	7,2193
n	0.8761	2.0644
R^2	0.9506	0.9423
Temkin isotherm		
K_T (L/mg)	1.0029	1.0016
B_1	60.649	22.682
R^2	0.9477	0.9085
b_t (J/mol)	40.851	109.23
Dubinin–Radushkevich isotherm		
q_D (mg/g)	173.0	78.48
B_D (mol^2/kJ^2)	0.0113	0.0037
R^2	0.9648	0.9017
E (kJ/mol)	6.6533	11.6279
Desorption parameter by 0.01 mol/L HNO_3		
Q_e (mg/g)	45.22	44.68
Q_d (mg/g)	<0.02	21.28
% desorption	–	47.68

where C_0 denotes the highest initial adsorbate concentration (mg/L). If $R_L = 1$, the process is assumed to be linear and if $R_L = 0$, it is expected to be irreversible (Emamy *et al.* 2021). The process is favorable if $0 < R_L < 1$, but unfavorable if $R_L > 1$ (Heidari *et al.* 2021; Lala *et al.* 2023). In this analysis, R_L revealed that Cr(VI) and Pb(II) adsorption onto MKL were favorable, with values of 0.58 and 0.15, respectively. Based on the high correlation coefficients (0.9822 for Cr(VI) and 0.957 for Pb(II)), the Langmuir isotherm model seems a suitable fit for the experimental data. The maximum monolayer Cr(VI) and Pb(II) adsorption capacities for MKL are 213 and 89 mg/g, respectively.

The Freundlich isotherm – Equation (6) – is used to analyze adsorption data for multiple layers with different adsorption energies:

$$\ln q_e = \frac{1}{n} \ln C_e + \ln K_F \tag{6}$$

where K_F is the Freundlich constant correlated to the biosorbent adsorption capacity and $1/n$ is the Freundlich constant ascribed to the adsorption intensity. Validation of the Freundlich isotherm required the use of a graph depicting ln q_e and ln C_e (Nkutha *et al.* 2021; Mardiah *et al.* 2022). The K_F and n values ascertained from the intercept and slope of Figure 2(b) are presented in Table 1. Based on the correlation coefficients (0.9506 for Cr(VI) and 0.9423 for Pb(II)), the experimental data appear to align well with the Freundlich isotherm model. The model's n values determine the nonlinearity between concentration and adsorption, offering insight into sorption favorability (Lim *et al.* 2019). Generally, the sorption characteristics are good when n is between 2 and 10. If it is between 1 and 2, it is moderately strict, and if it is below 1, sorption is deficient. The value of n for Cr(VI) adsorption was 0.87, indicating poor characteristics. It exceeded 2 for Pb(II), indicating that the ions are adsorbed favorably by MKL.

The Temkin isotherm model helps to understand material behavior. The model assumes that the adsorption heat of all molecules decreases linearly with the increase in the coverage of the adsorbent surface, and that

adsorption is characterized by a uniform distribution of binding energies, up to a maximum binding energy (Sahoo & Prelot 2020). The linear form of the Temkin isotherm model is shown in Equation (7):

$$q_e = B_1 \ln K_T + B_1 \ln C_e \tag{7}$$

where $B_1 = RT/b_t$, R is the universal gas constant, T is the absolute temperature at 298 K, the variable b_t is connected to the heat of adsorption (J/mol), and the Temkin adsorption potential (K_T) is measured in L/mg. Figure 2(c) shows the plots of q_e versus ln C_e, which depict Cr(VI) and Pb(II) adsorption onto the MKL biosorbent. Table 1 shows the values of K_T and B_1, which were obtained by calculating the slope and intercept of the q_e versus ln C_e plots. Based on the high correlation coefficients of 0.9477 for Cr(VI) and 0.9085 for Pb(II), it can be concluded that the Temkin model provides a suitable fit for the experimental data. The values of b_t of Cr(VI) and Pb(II) adsorption were determined as 40.85 and 109.23 J/mol, respectively. Studies indicate that heats of sorption below 20 kJ/mol are characteristics of physisorption (Lim *et al.* 2019; Emamy *et al.* 2021). The low b_t value, in this case, suggests a weak link to the MKL, indicating physical adsorption (Ali *et al.* 2019; Azizi *et al.* 2023).

The Dubinin–Radushkevich isotherm model can distinguish between chemical and physical adsorption, describing how adsorbates are adsorbed, and is used to calculate the energy required for the absorption process (Mehrmand *et al.* 2022; Abadi *et al.* 2023). The linearized model is given by Equation (8):

$$\ln q_e = \ln q_D - 2B_D\varepsilon \tag{8}$$

and

$$\varepsilon = RT \ln\left(1 + \frac{1}{C_e}\right) \tag{9}$$

where q_D is the adsorbent's maximum adsorption capacity (mg/g); B_D (mol^2/kJ^2) is the adsorption energy constant; andε is the Polanyi potential (Ali *et al.* 2019; Abadi *et al.* 2023). The values of B_D and q_D (Table 1) were defined from the intercept and slope of ln q_e versus RT ln $(1 + 1/C_e)$ (Figure 2(d)). The correlation coefficients for Cr(VI) and Pb(II) adsorption are 0.9648 and 0.9017, indicating that the experimental data align well with the model.

The average adsorption energy required can be estimated using Equation (10):

$$E = (2B_D)^{-1/2} \tag{10}$$

The value of E can give information about how adsorption occurs. The energy required when transferring one mole of ions can determine the adsorption process (Mehrmand *et al.* 2022). Between 1 and 8 kJ/mol, it is physisorption; between 8 and 16 kJ/mol, it is adsorption followed by ion exchange, while 20–40 kJ/mol indicates chemisorption. The 6.65 kJ/mol for Cr(VI) suggests physisorption (Ali *et al.* 2019; Mehrmand *et al.* 2022). The value of E for Pb(II) adsorption is 11.62 kJ/mol, indicating ion exchange.

3.6. Adsorption kinetics

To gain a better consideration of the adsorption rate of Cr(VI) and Pb(II) by MKL within a specific time, several kinetic models were examined: pseudo-first-order, pseudo-second-order, and intra-particle diffusion (Arrisujaya *et al.* 2019; Lala *et al.* 2023). The results for constant rate studies for various initial concentrations of adsorbate solution (Cr(VI) or Pb(II)) by all kinetic models are listed in Table 2. The pseudo-first-order kinetic model is founded on the idea that the rate of solute absorption increases with time in proportion to the variation between the level of saturation concentration and the quantity of solid uptake during a specific duration remains an essential factor (Sahoo & Prelot 2020; Shooto 2020). The kinetic model commonly represents the initial stage of adsorption. The pseudo-first order kinetic model is represented by Equation (11):

$$\frac{dq_t}{dt} = K_1(q_e - q_t) \tag{11}$$

Table 2 | Kinetic model rate constants for Cr(VI) and Pb(II) adsorption onto MKL

	Pseudo-first order			Pseudo-second order			Intra-particle diffusion		
Adsorbate Cr(VI) (mg/L)	K_1 (min^{-1})	q_{e1} (mg/g)	R^2	K_2 (g/(mg min))	q_{e2} (mg/g)	R^2	k_i	C_i	R^2
50	2.1991	42.37	0.629	0.0139	42.01	0.998	0.3824	37.582	0.5371
100	5.5593	84.74	0.739	0.0011	89.28	0.994	2.1363	59.721	0.9143
150	38.926	147.05	0.992	0.0001	142.85	0.996	8.2395	22.18	0.9473
Pb(II) (mg/L)									
50	2.8652	31.34	0.276	0.0037	33.67	0.991	0.5682	25.176	0.5653
100	3.6862	39.21	0.599	0.0051	38.31	0.993	0.8079	48.795	0.6436
150	14.277	50.5	0.953	0.0012	48.78	0.997	7.0489	129.26	0.9458

The chemisorption step limits the adsorption rate by the pseudo-second-order model (Figure 3(a) and 3(d)). The kinetic model of this form can possess adsorption behavior across the complete range. The pseudo-second-order kinetic model is represented by Equation (12):

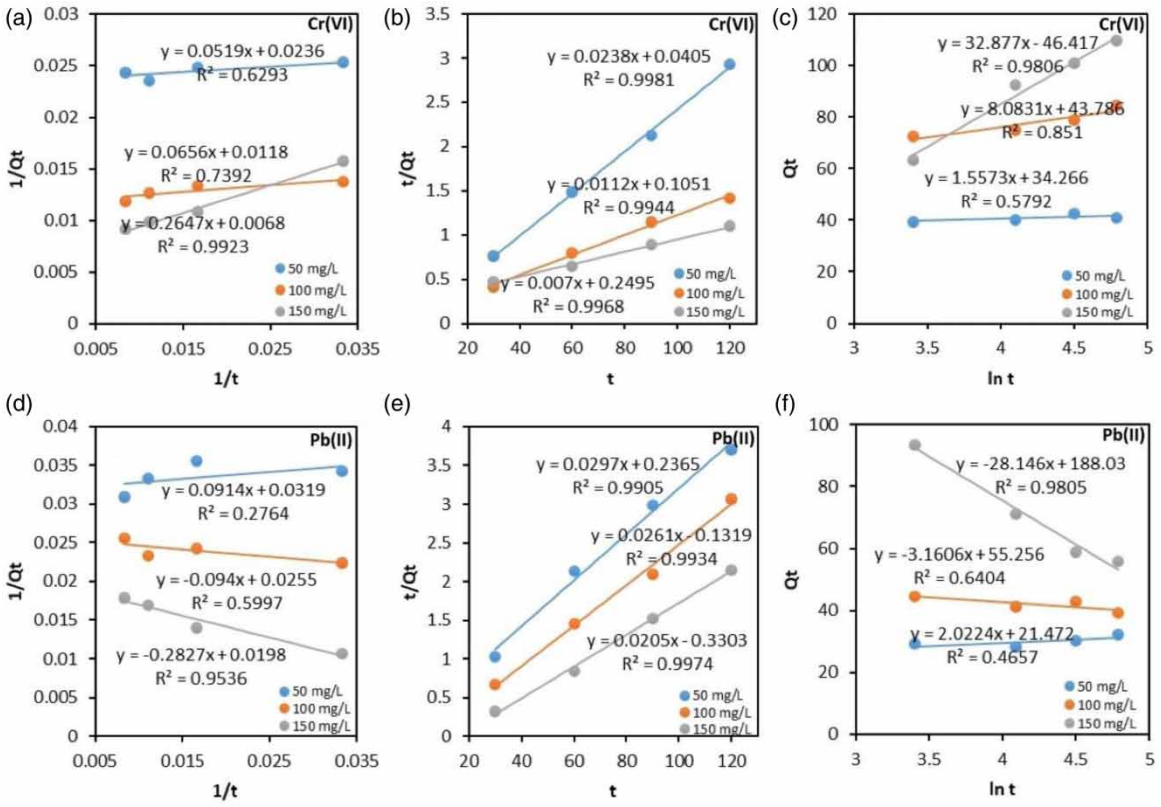

Figure 3 | Adsorption kinetic models for Cr(VI) and Pb(II) using MKL. (a) and (d) Pseudo-first order; (b) and (e) pseudo-second order; and (c) and (f) intra-particle diffusion.

$$\frac{t}{q_t} = \frac{1}{K_2 q_e^2} + \frac{t}{q_e} \tag{12}$$

where K_2 is the equilibrium rate constant of the pseudo-second-order model (g/mg min), at all initial concentrations of Cr(VI) and Pb(II) studied, very high correlation coefficients (>0.99) were obtained working with

the pseudo-second-order kinetic model (Figure 3(b) and 3(e)). K_2 decreases as Cr(VI) concentration increases for the MKL biosorbent in Table 2. This behavior arises because of reduced adsorption competition on surface sites at low concentrations. The K_2 value for Pb(II) adsorption is frequently lower than that of Cr(VI), indicating more rapid adsorption of Cr(VI) by MKLs.

Weber and Morris developed an intra-particle mass transfer diffusion model to determine diffusion in adsorption (Sahoo & Prelot 2020). The model is expressed by Equation (13):

$$q_t = k_i t^{0.5} + C_i \tag{13}$$

where k_i is the rate of intra-particle diffusion (mg/g $min^{-1/2}$), and the rate constants k_i and C_i (mg/g) are determined from the slope and intercept of the regression line (the plots of q_t as a function of $t^{0.5}$). To determine the boundary layer thickness accurately, it is essential to analyze the C values thoroughly, high values indicate more significant boundary layer effects. The linear plot's intercept (Figure 3(c) and 3(f)) suggests that absorption involves more than intra-particle diffusion as a rate-controlling step (Sahoo & Prelot 2020). The process is complex and includes multiple diffusion resistances, implying that the surface biosorbent worked simultaneously with intra-particle diffusion (Shooto 2020) in the adsorbate and MKL interactions.

3.7. Temperature effect and thermodynamic studies

The effect of temperature at 303, 308, and 313 K for the adsorption of Cr(VI) and Pb(II) ions onto MKL is shown in Figure 4. The adsorption capacity of MKL toward Cr(VI) ions increased when the temperature was raised from 303 to 313 as shown in Figure 4. This is significant because it shows that high temperatures give the metal ions in the solution the kinetic energy necessary to overcome all factors impeding the adsorption processes. This was caused by an enhanced diffusion rate. This demonstrated that the adsorption processes were endothermic. However, the adsorption of Pb(II) slightly decreased when the temperature of the system was increased. The adsorption of Pb(II) decreased with increased temperature of the system; this suggested that the reactions were exothermic in nature.

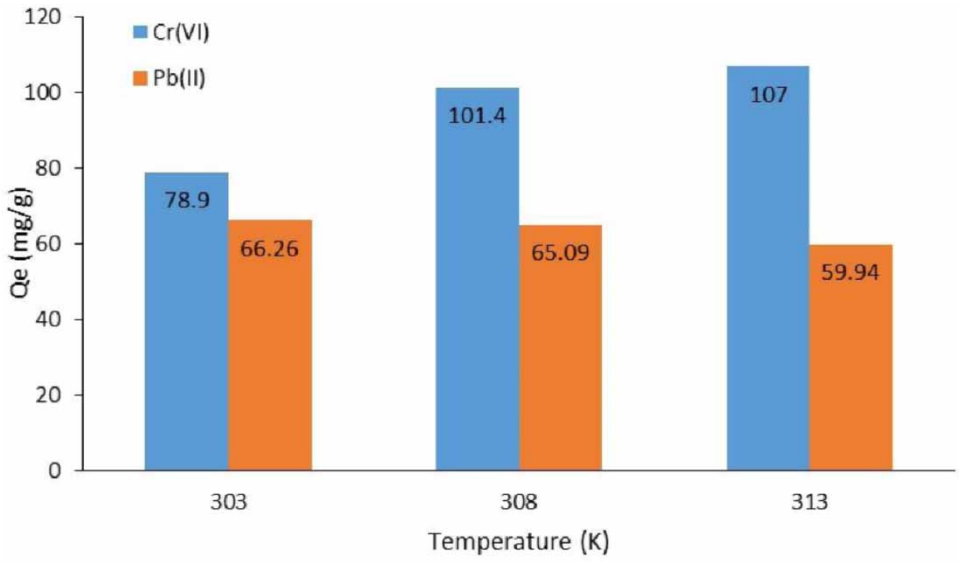

Figure 4 | Temperature effect on the adsorption of Cr(VI) and Pb(II) ions onto MKL.

To analyze adsorption thermodynamics, equilibrium constants and thermodynamic parameters that vary with temperature must be calculated, including the Gibbs free energy (ΔG), enthalpy (ΔH), and entropy (ΔS) (Hevira *et al.* 2020). These can be determined using Equations (14)–(16) inclusive:

$$\Delta G = -RT\ln K_L \tag{14}$$

$$K_L = C_0 - C_e/C_e \tag{15}$$

$$\Delta G = \Delta H - T\Delta S \tag{16}$$

ΔH and ΔS were determined from the slope and intercept of the linear plot of ΔG versus T. Figure 5 shows the thermodynamic parameters obtained. The negative values of ΔG confirm that Cr(VI) adsorption by MKL is favorable and spontaneous (Tangtubtim & Saikrasun 2019). The Gibbs free energy values for Pb(II) adsorption are positive, however, and it is noted that the adsorption process is non-spontaneous (Shooto 2020). The positive value of ΔG also indicates that there is an energy barrier.

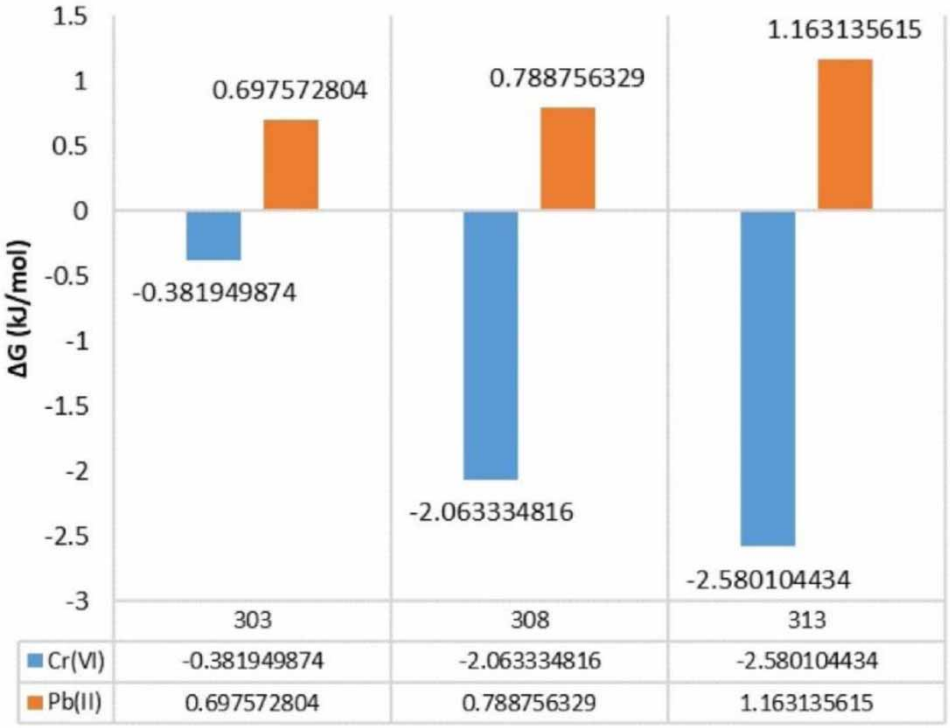

Figure 5 | Thermodynamic parameters for Cr(VI) and Pb(II) adsorption by MKL (Cr(VI) ΔH: 66.028 kJ/mol, ΔS: 219.8 J/mol K and Pb(II) ΔH: −13.456 kJ/mol, ΔS: −46.6 J/mol K).

The values of ΔH for Cr(VI) are positive, indicating that adsorption is endothermic (Tangtubtim & Saikrasun 2019; Shooto 2020), while Pb(II) adsorption on MKL is exothermic (i.e., $\Delta H < 0$) (Komárek *et al.* 2015). The positive value of ΔS suggests an increase in disorder during Cr(VI) adsorption onto MKL at the solid/solution interface. A negative entropy change for Pb(II) adsorption shows a decrease in entropy, and the system converts less randomly (Azizi *et al.* 2023). Physisorption has an energy change range of −20 to 0 kJ/mol, while that for chemisorption it is from −80 to −400 kJ/mol (Shooto 2020). This study shows that the values of ΔG do not indicate chemisorption or physisorption, but rather, different adsorption processes like ion exchange with exchangeable cations or surface complexation (Nkutha *et al.* 2021) with binding sites on MKLs.

3.8. Comparative studies on Cr(VI) and Pb(II) adsorption

This study's findings suggest that MKL can potentially serve as a valuable biosorbent for Cr(VI) and Pb(II) (Table 3).

3.9. Desorption

Desorption studies aid in explaining the process of adsorbate adsorption. In the adsorption–desorption experiments, 0.01 mol/L of HNO_3 was used for a single cycle, which is considered inadequate. The desorption efficiency result is given in Table 1. The studies show that Cr(VI)-loaded MKL was not desorbed by 0.01 mol/L HNO_3 (pH 2), while about 48% of Pb(II) was desorbed from loaded MKL. Cr(VI) does not affect the desorption solution at pH 2. The desorption solution works well with Pb(II) at pH 2, however. Accordingly, nitric acid selected in this study is believed to play functions in both desorption and protonation. This desorption study

Table 3 | Comparing the maximum adsorption capacity of different natural adsorbent materials

Adsorbents	Adsorbates	q_{max} (mg/g)	pH	Dosage (g/L)	Reference
Sweet flag	Cr(VI)	24.48	1.0	0.2	Shooto (2020)
Juniperus procera leaves	Cr(VI)	23	4.0	10	Ali *et al.* (2019)
Green tea leaves	Cr(VI)	26.39	2.0	40	Jeyaseelan & Gupta (2016)
Areca nut leaf sheath	Cr(VI)	109.89	2.0	1.25	Pant *et al.* (2022)
Rice husk	Cr(VI)	42.37	2.0	40	Lala *et al.* (2023)
MKL	Cr(VI)	213	2.0	1.0	This work
Sweet flag	Pb(II)	88.08	8.5	0.2	Shooto (2020)
Juniperus procera leaves	Pb(II)	30.3	4.6	10	Ali *et al.* (2019)
Pomelo leaves	Pb(II)	207.2	4.0	2.0	Lim *et al.* (2019)
Lawsonia Inermis	Pb(II)	15.41	5.0	5.0	Mehrmand *et al.* (2022)
Pineapple fiber	Pb(II)	165	5.0	0.1	Tangtubtim & Saikrasun (2019)
MKL	Pb(II)	89	6.0	1.0	This work

considered the degree of acidity or alkalinity of the desorption solution, affecting the high acid/base concentrations. The desorption study had previously considered the desorption solution's degree of acidity or alkalinity, which significantly varied the acid or base concentration. Each adsorbate may be more or less appropriate for the acidity or basicity of the desorption solution.

4. CONCLUSIONS

The study aimed to examine the potential effectiveness of using MKLs in removing Cr(VI) and Pb(II) ions from aqueous solutions. Cr(VI) and Pb(II) adsorptions onto MKLs were based on adsorbate solution pH, biosorbent dosage, contact time, initial adsorbate concentrations, and temperature. The adsorption equilibrium data fit the Langmuir, Freundlich, Temkin, and Dubinin–Radushkevich isotherm models adequately.

As per the Langmuir model, the maximum MKL adsorption capacities of Cr(VI) at pH 2 and Pb(II) at pH 6 were approximately 213 and 89 mg/g, respectively. The Langmuir isotherm R_L values for MKLs for Cr(VI) and Pb(II) indicate a favorable process. The Freundlich isotherm n values showed that Cr(VI) adsorption had poor adsorption characteristics, while Pb(II) was adsorbed favorably by MKLs. The value of b_t for the Temkin isotherm for Cr(VI) and Pb(II) adsorption was characteristic of physisorption. The E values for the Dubinin–Radushkevich isotherm show that the Cr(VI) adsorption by MKL was physisorption, while that of Pb(II) was chemisorption.

The pseudo-second-order kinetic model was the most suitable for Cr(VI) and Pb(II) adsorption in the kinetic study. The adsorption kinetic studies show that chemisorption may explain the process, including valency forces through sharing or exchanging electrons for Cr(VI) and Pb(II) on MKLs. The removal of Cr(VI) onto MKL was favored at high temperatures while Pb(II) favored low temperature. Thermodynamic analysis studies revealed that surface complexation coexisted with ion exchange as the primary removal mechanism.

ACKNOWLEDGEMENTS

This work was financially supported in part by Research and Community Service Institution (LP2M), Universitas Nusa Bangsa, Indonesia, by Research Contract Number: 098/REK-UNB/SPK/VIII/2022, the fiscal year 2022.

DATA AVAILABILITY STATEMENT

All relevant data are included in the paper or its Supplementary Information.

CONFLICT OF INTEREST

The authors declare there is no conflict.

REFERENCES

Abadi, B. F. R., Arrisujaya, D., Nurlela, N. & Wardhani, G. A. P. K. 2023 A comparison study of Rhodamine B adsorption using acid-base-activated *Hura crepitans* L. fruit carpel. *Jurnal Litbang Industri* **13**(1), 11.

Ali, I. H., Al Mesfer, M. K., Khan, M. I., Danish, M. & Alghamdi, M. M. 2019 Exploring adsorption process of lead (II) and chromium (VI) ions from aqueous solutions on acid activated carbon prepared from *Juniperus procera* leaves. *Processes* **7**(4), 217.

Arrisujaya, D., Ariesta, N. & Maslahat, M. 2019 Removal of chromium (VI) from aqueous solutions using *Diospyros discolor* seed activated with nitric acid: isotherm and kinetic studies. *Water Science and Technology* **79**(6), 1214–1221.

Arrisujaya, D., Susanty, D. & Hastuti, L. T. 2020 The effect of three variants of extracting solvents on the total phenolic content and antioxidant activity of *Diospyros blancoi* seeds. *International Journal of Fruit Science* **20**(Suppl 3), S1192–S1200.

Azizi, A., Forghani, M., Kafshgari, L. A. & Hassanzadeh, A. 2023 Adsorptive removal behavior of Pb (II) and Cr (VI) pollutants from an aqueous environment onto polyaniline-modified MIL100(Fe). *Minerals* **13**(3), 299.

Darsono, B. S., Hikmat, A. & Soekmadi, R. 2022 Ethnobotany of Kemang (*Mangifera kemanga* Blume.) as identity flora of Bogor Regency. *Media Konservasi* **27**(2), 34–41.

Emamy, F. H., Bumajdad, A. & Lukaszewicz, J. P. 2021 Adsorption of hexavalent chromium and divalent lead ions on the nitrogen-enriched chitosan-based activated carbon. *Nanomaterials* **11**(8), 1907.

Heidari, A., Sayadi, M. H. & Biglari Quchan Atigh, Z. 2021 A comparative study of different materials (drinking water treatment sludge, nanoclay, and modified nanoclay) for simultaneous removal of hexavalent chromium and lead. *International Journal of Environmental Science and Technology* **18**(11), 3553–3570.

Hevira, L., Zilfa, R., Ighalo, J. O. & Zein, R. 2020 Biosorption of indigo carmine from aqueous solution by *Terminalia catappa* shell. *Journal of Environmental Chemical Engineering* **8**(5), 104290.

Jeyaseelan, C. & Gupta, A. 2016 Green Tea Leaves as a Natural Adsorbent for the Removal of Cr(VI) from Aqueous Solutions. *Air, Soil and Water Research* **9**, ASWR.S35227.

Komárek, M., Koretsky, C. M., Stephen, K. J., Alessi, D. S. & Chrastný, V. 2015 Competitive adsorption of Cd(II), Cr(VI), and Pb(II) onto nanomaghemite: a spectroscopic and modeling approach. *Environmental Science & Technology* **49**(21), 12851–12859.

Lala, M. A., Ntamu, T. E., Adesina, O. A., Popoola, L. T., Yusuff, A. S. & Adeyi, A. A. 2023 Adsorption of hexavalent chromium from aqueous solution using cationic modified rice husk: parametric optimization via Taguchi design approach. *Scientific African* **20**, e01633.

Lim, L. B. L., Priyantha, N., Lu, Y. & Zaidi, N. A. H. M. 2019 Adsorption of heavy metal lead using *Citrus grandis* (Pomelo) leaves as low-cost adsorbent. *Desalination and Water Treatment* **166**, 44–52.

Lin, C., Li, S., Chen, M. & Jiang, R. 2017 Removal of Congo red dye by gemini surfactant C_{12}-4-C_{12} · 2Br-modified chitosan hydrogel beads. *Journal of Dispersion Science and Technology* **38**(1), 46–57.

Mardiah, S. H., Arrisujaya, D., Susanty, D. & Yuliani, N. 2022 Preparation, characterization and phenol adsorption of *Mangifera kemanga* Blume seed. *Jurnal Sains Natural* **12**(3), 103–111.

Mehrmand, N., Moraveji, M. K. & Parvareh, A. 2022 Adsorption of Pb(II), Cu(II) and Ni(II) ions from aqueous solutions by functionalised henna powder (*Lawsonia inermis*): isotherm, kinetic and thermodynamic studies. *International Journal of Environmental Analytical Chemistry* **102**(1), 1–22.

Nazaruddin, N., Arrisujaya, D., Hidayat, H., Zein, R., Munaf, E. & Jin, J. 2014 Batch method for the removal of toxic metal from water using sugar palm fruit (*Arenga pinnata* Merr) shell. *Research Journal of Pharmaceutical Biological and Chemical Sciences* **5**(2), 1619–1629.

Nkutha, C. S., Naidoo, E. B. & Shooto, N. D. 2021 Adsorptive studies of toxic metal ions of Cr(VI) and Pb(II) from synthetic wastewater by pristine and calcined coral limestones. *South African Journal of Chemical Engineering* **36**, 43–57.

Pant, B. D., Neupane, D., Paudel, D. R., Chandra Lohani, P., Gautam, S. K., Pokhrel, M. R. & Poudel, B. R. 2022 Efficient biosorption of hexavalent chromium from water by modified arecanut leaf sheath. *Heliyon* **8**(4), e09283.

Sahoo, T. R. & Prelot, B. 2020 Adsorption processes for the removal of contaminants from wastewater. In: *Nanomaterials for the Detection and Removal of Wastewater Pollutants*. Elsevier, pp. 161–222. Available from: https://linkinghub.elsevier.com/retrieve/pii/B9780128184899000074 (accessed 13 July 2023).

Shooto, N. D. 2020 Removal of toxic hexavalent chromium (Cr(VI)) and divalent lead (Pb(II)) ions from aqueous solution by modified rhizomes of Acorus calamus. *Surfaces and Interfaces* **20**, 100624.

Tangtubtim, S. & Saikrasun, S. 2019 Effective removals of copper (II) and lead (II) cations from aqueous solutions by polyethyleneimine-immobilized pineapple fiber. *Bioresource Technology Reports* **7**, 100188.

First received 24 July 2023; accepted in revised form 17 October 2023. Available online 28 October 2023